HHS Public Access

Author manuscript

Int J Radiat Oncol Biol Phys. Author manuscript; available in PMC 2022 November 01.

Published in final edited form as:

Int J Radiat Oncol Biol Phys. 2021 November 01; 111(3): 671–683. doi:10.1016/j.ijrobp.2021.06.001.

First Multimodal, Three-Dimensional, Image-Guided Total Marrow Irradiation Model for Preclinical Bone Marrow Transplantation Studies

Darren Zuro, (MS)[1,*], **Srideshikan Sargur Madabushi, (PhD)**[1,*], **Jamison Brooks, (BS)**[1], **Bihong T. Chen, (MD, PhD)**[2], **Janagama Goud, (PhD)**[1], **Amandeep Salhotra, (MD)**[3], **Joo Y. Song, (MD)**[4], **Liliana Echavarria Parra, (BS)**[1], **Antonio Pierini, (MD, PhD)**[5], **James F Sanchez, (PhD)**[6], **Anthony Stein, (MD)**[3], **Monzr Al Malki, (MD)**[3], **Marcin Kortylewski, (PhD)**[7], **Jeffrey Y.C. Wong, (MD)**[1], **Parham Alaei, (PhD)**[8], **Jerry Froelich, (MD)**[9], **Guy Storme, (MD, PhD)**[10], **Susanta K Hui, (PhD)**[1,6,8,§]

[1]Department of Radiation Oncology, City of Hope Medical Center, Duarte, CA

[2]Department of Diagnostic Radiology, City of Hope Medical Center, Duarte, CA

[3]Department of Hematology and HCT, City of Hope Medical Center, Duarte, CA

[4]Department of Pathology, City of Hope Medical Center, Duarte, CA

[5]Division of Hematology and Clinical Immunology, Department of Medicine, University of Perugia, Perugia, Italy

[6]Beckman Research Institute of City of Hope, Duarte, CA

[7]Department of Immuno-Oncology, Beckman Research Institute, City of Hope, Duarte, CA, USA;

[8]Department of Radiation Oncology, University of Minnesota, Minneapolis, USA

[9]Department of Radiology, University of Minnesota, Minneapolis, MN

[10]Department of Radiotherapy UZ Brussel, Laarbeeklaan, 101, 1090-Brussel, Jette, Belgium

Abstract

Purpose: Total marrow irradiation (TMI) has significantly advanced radiation conditioning for hematopoietic cell transplantation in hematological malignancies by reducing conditioning-

[§]***Corresponding Author:Susanta Kumar Hui***, Professor, Department of Radiation Oncology, City of Hope Medical Center, 1500 E Duarte Rd, Duarte, CA 91010, Tel. 626-218-0556; shui@coh.org.

Authors Responsible for Statistical Analysis

Darren Zuro (dzuro@coh.org)

Srideshikan Sargur Madabushi (smadabushi@coh.org)

[*]These authors made an equal contribution to the manuscript

Conflict of Interest

Susanta K Hui receives honoraria from and consults for Janssen Research & Development, LLC. Anthony Stein provides consulting for Amgen and Stemline and is on the speakers' bureau for the former company. All other authors declare no competing financial interests

induced toxicities and improving survival outcomes in relapsed/refractory patients. However, the relapse rate remains high, and the lack of a preclinical TMI model has hindered scientific advancements. To accelerate TMI translation to the clinic, we developed a TMI delivery system in pre-clinical models.

Methods: A Precision X-RAD SmART irradiator was used for TMI model development. Images acquired by whole-body contrast-enhanced computed tomography (CT) were used to reconstruct and delineate targets and vital organs for each mouse. Multiple beam and CT-guided Monte Carlo-based plans were performed to optimize doses to the targets and to vary doses to the vital organs. Long-term engraftment and reconstitution potential were evaluated by a congenic bone marrow transplantation (BMT) model and serial secondary BMT, respectively. Donor cell engraftment was measured using non-invasive bioluminescence imaging (BLI) and flow cytometry.

Results: Multimodal imaging enabled identification of targets (skeleton and spleen) and vital organs (e.g., lungs, gut and liver). In contrast to total body irradiation (TBI), TMI treatment allowed variation of radiation dose exposure to organs relative to the target dose. Dose reduction mirrored that in clinical TMI studies. Similar to TBI, mice treated with different TMI regimens showed full long-term donor engraftment in primary BMT and second serial BMT. The TBI-treated mice showed acute gut damage, which was minimized in mice treated with TMI.

Conclusion: A novel multimodal image guided preclinical TMI model is reported here. TMI conditioning maintained long-term engraftment with reconstitution potential and reduced organ damage. Therefore, this TMI model provides a unique opportunity to study the therapeutic benefit of reduced organ damage and BM dose escalation to optimize treatment regimes in BMT and hematological malignancies.

Introduction

Hematopoietic cell transplantation (HCT) is a curative treatment option for several malignant and non-malignant hematological diseases. For over half a century, total body irradiation (TBI) has been a standard of care as a preconditioning regimen for host immune suppression and reduction of disease burden to allow donor engraftment(1,2). However, pulmonary toxicities(3,4) and acute graft-vs-host disease (GVHD) are a major post-transplantation complication(5). Although increased radiation and chemotherapy may reduce the leukemia burden(6), mortality from high-dose toxicities offsets any improvements in relapse rates(7). To overcome these limitations, a whole body computed tomography (CT) image-guided total marrow irradiation (TMI) modality for clinical use(8) was developed, which delivers radiation to the entire skeletal system and other potential sites of disease (e.g., lymph node, testis) while limiting radiation exposure to vital organs. Recent studies showed that dose-escalated TMI (20 Gy) as a preparative regimen prior to allogenic HCT for high-risk refractory leukemia patients increased therapeutic benefit, conferring an overall survival (OS) rate of 48% at 2 years(9), in contrast to the <10% OS reported for similar patients with active disease given TBI- or busulfan-based myeloablative regimens(10). However, relapse remains a major problem, suggesting more research is needed to optimize TMI treatment for improving the survival benefit of patients with relapsed/refractory AML and to explore combinatorial therapeutics including TMI together with immunomodulatory drugs for hematological diseases(11,12).

Although clinical TMI technological development has led to a large number of clinical trial investigations worldwide to allow dose escalation and reduction of relapse for patients with high-risk leukemia(13–16), a lack of advanced pre-clinical technology has limited the scope of further scientific advances. The conventional mouse TBI treatment(17) lacked imaging identifying organs, as well as a 3D dosimetric model to calculate detailed organ dosimetry, and ignored the dosimetric effect of tissue heterogeneity. A film-based 2D image guidance identifying organ position and copper compensator was used to develop the first-generation preclinical TMI(18). However, it lacks 3D imaging to detect target and organs, generating organ dosimetry such as dose volume histograms (DVH), inclusion of tissue heterogeneity, and ability to vary dose exposures. Therefore, there is an unmet need for the development of a 3D image guided preclinical TMI treatment model.

We report here the development of an image-guided, high-precision preclinical TMI mouse model and evaluate its potential for maintaining long-term bone marrow engraftment while reducing organ damage, in comparison to standard preclinical TBI. Previous efforts to reduce whole-body radiation with the aim of reducing toxicity have resulted in increased relapse potential (19), and reduced engraftment or mixed chimerism(20), which can be overcome by increasing the number of donor cells(21). However, it is unknown how varying radiation exposure to vital organs could affect engraftment dynamics. Since TMI can maintain a high dose of radiation to the bone marrow and spleen, we hypothesized that TMI, along with reduced radiation exposure to body, will allow successful long-term engraftment. We further explored a comparative evaluation of TMI dosimetry between preclinical models and clinical data.

Methods and Materials

TMI treatment workflow

A workflow for TMI planning and treatment is represented in Fig. 1. The TMI treatment was performed using the X-ray irradiator (Precision X-Ray, North Branford, CT, USA) in compliance with current guidelines(22). The major steps involved are explained below.

1) Treatment positioning—An air-tight animal holder (6” long, cylindrical) made primarily of Delrin® and acrylic material was constructed. The animal was placed in a custom designed animal holder under isoflurane anesthesia to ensure reproducible animal positioning and immobilization. A built-in laser system and scout image (fast partial CT) were used for alignment and verification purposes. The holder limits animal motion along the longitudinal axis, increasing positioning reproducibility. Two ports from the front of the holder allowed circulation of isoflurane for anesthesia.

2) Whole body cone-beam computed tomography (CBCT) imaging to identify target and vital organs—To verify beam coverage of the entire spleen and to provide dose estimations to other soft tissues in the treated mice, a subset of mice were imaged using iodine-based eXIA™ 160 contrast agent as a soft tissue contrast agent to visualize and contour organs(23,24). The eXIA™ 160 (Binitio Biomedical Inc, Ottawa, Canada) agent was injected (0.1 mL (~16 mg Iodine)/20g mice) intravenously via the tail vein. Mice were imaged before injection and at 1 h, 4h, and 24h post injection to measure the temporal

pattern of contrast enhancement. Mice images without contrast agents were registered to images of mice with contrast using Velocity software (Varian Medical Systems, Inc, Palo Alto, CA, USA). Using Velocity, sensitive soft tissue organs were identified and contoured for use in treatment planning. Additionally, whole body microMRI (MR solution, Guildford, United Kingdom) was performed in five mice, and co-registered with a CT scan using Velocity to verify position of organs (Supplementary Fig S1C). Organs were hand-contoured by the operator, and a board-certified radiologist (B.T.C) evaluated images and contours.

3) TMI treatment planning and analysis—Mouse CT scans were divided into seven regions for treatment optimization. Radiation beam layout by regions (beam size, isocenter location, normalization point) is provided in Supplementary Table S1. For each region, parallel opposed beams with varied beam size were used to create a homogenized dose within the center of the beams. Visualization of a projected radiation beam on a 3D CT image allowed for adjustment of beam size and isocenter to cover the target and reduce exposure to adjacent critical organs. To plan the TBI treatments, three regions with parallel opposed beams (40X40 mm^2 square beams size) were used to cover dose exposure to the body at 11 Gy, with the dose normalized to the center of the animal's body. Various TMI planning options were generated for survival and engraftment studies as described later. CT-guided Monte Carlo dose calculation were performed using SmART-Plan(25) with vendor recommended settings (Supplementary Table S2) (26,27).

4) TMI treatment delivery—Mice were treated in the prone position. After creation of the TMI treatment plan, an individual mouse (placed in mouse holder under anesthesia) was repositioned on the center of table, guided by laser alignment as described earlier for image scanning, to match the planning reference animal. CBCT or scout images of the treated mice were acquired and co-registered to the reference planning mouse using on-board registration software. Both TBI and TMI were delivered at the isocenter with a dose rate approximately 400 cGy/minute. The total treatment time for an 11 Gy TMI treatment was approximately 60 minutes. We further measured the effect of (a) mouse positioning (prone and supine) and (b) animal sizes weighing 16-18g, 19-22g, and 29-31 g on TMI dosimetry.

Dosimetric validation

Detailed validation of Monte Carlo-based treatment planning system (TPS) including calculation of dose-to-medium were previously published(22,25). Additional dosimetric validation was performed using the following steps: (i) Film and dosimeter-based dosimetry: The Gafchromic™ EBT3 films placed on the table underneath a mouse (laying on its sagittal plan) at three different regions (spine, lungs, and gut) and CBCT was obtained. Two Gy radiation was delivered perpendicularly to the animal's sagittal plane. The mean dose measurement from film was compared with mean exit dose calculated to the film using CBCT-guided TPS. A similar process was adopted for verifying the exit dose of 5 Gy on optically stimulated luminescent dosimeters (OSLDs).

Secondary dose simulation of bone and marrow: Due to the small size of mouse bone (~2mm), it is difficult to evaluate characteristics of the dose profile in bone, marrow, and their junction. Therefore, we fabricated a large 3D cylindrical biocompatible bone and

marrow mimetic phantom to simulate the dose profile across the two mediums and their junctions. The average Hounsfield unit (HU) of the bone material was measured to be 996 ±130 which is within the range of normal bone density values. A parallel opposed beam (20X20 mm^2) was used from the side, and the dose was normalized (11 Gy) at the center (water, bone marrow equivalent) of the phantom. Further detail is available in the dosimetry section of the supplement.

Survival study

Mice were randomly distributed to different groups, exposed to different regimens and followed for survival. TBI (11 Gy), TMI I (11 Gy), TMI 12 Gy and TMI 14 Gy were delivered in single fraction, while TBI, TMI I, TMI I+4, TMI I+6 and TMI 14 Gy were delivered in two fractions at 6h difference. Mice were then followed for survival.

TMI treatment plans used for assessment of engraftment in a congenic BMT model

A congenic BMT model was carried out by transplanting donor C57BL/6 (CD45.2) BM cells in irradiated recipient CD45.1 B6 mice. For initial TMI-based engraftment assessment, 4 separate treatment plans (TMI I, TMI I+2, TMI I+4, and TMI I+6) were generated. TMI I is the treatment plan where the bones receives the prescription dose (11 Gy) while the rest of the body receives as low as reasonably achievable dose (this dose is due to their proximity to the beams placed in TMI plan). TMI I+2, TMI I+4 and TMI I+6 are treatment plan where mice are deliberately treated with 2 Gy, 4 Gy and 6 Gy TBI respectively, and TMI doses were varied to maintain 11 Gy prescription dose to the bones. Alternative simplified description is following, (TMI I: TMI 11 Gy + TBI 0 Gy); (TMI I+2: TMI 9 Gy + TBI 2 Gy); (TMI I+4: TMI 7 Gy + TBI 4 Gy) and (TMI I+6: TMI 5 Gy + TBI 6 Gy). Subsequently, treatment was delivered (in two fractions, 6h difference) and engraftment differences was evaluated between different TMI treatments using bioluminescence imaging (BLI) and compared it with TBI (11 Gy). We selected two TMI treatment groups TMI I, and TMI I+4 for long-term engraftment and secondary bone marrow transplant studies. Three days post BMT, small intestines were harvested, and histological analysis was carried out. For non-invasive assessment of BM cells engraftment, whole body BLI imaging were performed. The details are in the supplementary method section.

Comparative evaluation of dose coverage between preclinical and clinical TMI

We reviewed published articles in which patients with leukemia were treated with TMI techniques using either helical Tomotherapy (Tomotherapy Inc, Madison, WI, USA) or volumetric arc therapy (VMAT) linear accelerators. Among the available literature, we selected 10 previously published papers on TMI to obtain Dosimetric coverage to various organs such as the skeleton, gut, lungs, kidneys, liver, and spleen.(13,28–34) Since prescription dose to target varies across centers, we tabulated the relative dose exposure to organs with respect to the prescribed dose and compared with the relative dose exposure obtained in our preclinical TMI model.

Results

Pre-imaging setup and identification of soft tissues and organs

Images of the custom-made treatment bed are presented in Fig. 2A–B. The absolute displacement was reduced from 2.8 ± 1.1 mm using the standard bed to 1.5 ± 0.7 mm using the customized holder (n=5). Temporal visualization of the contrast-enhanced CT images are shown in (Fig. 2C–F). Fig. 2G shows contrast uptake by different organs over time, suggesting that a CT image, one hour post contrast injection, will provide maximum contrast for organ delineation. Accordingly, 3D organs were contoured for treatment planning as shown in Fig. 2H.

Dosimetric validation of TMI

Fig. 3A displays a fluoroscopic image of a mouse with beam layout. Fig. 3B shows Gafchromic film exposed to the TMI plan. Fig 3C & D depicts dose measured on film and OLSD respectively for X rays passing through three regions displayed in red (spine (i), lungs (ii), and gut (iii)). Film and OSLD measurements were within ±5% accuracy of the simulated TMI dose calculation. *In vivo*, dose profiles of bone and marrow at two regions, femur and spine, are shown in Fig. 3 E&F. The dose profile for the BM phantom is shown in Fig. 3G. Both phantom and *in vivo* dose profile assessments revealed that the relative dose to the bone was 2.5 times higher than to the marrow dose (37 ± 3% n=5 mice, as compared to femoral bone). For example, when the bone marrow received an 11 Gy prescription dose, the mean dose absorption to the bone was approximately 27.5 Gy.

TMI treatment planning and dosimetry

Schematics with demonstrations for parallel opposed beams in coronal view (Fig. 4A), sagittal view (Fig. 4B) and in a representative two cross-sectional views (Fig. 4C & 4D) presented the beam layout for a TMI treatment. The details of different TMI treatment plans used in this study are mentioned in method sections. The 3D dose distributions represented by the DVHs are shown for TMI I, TMI I+4, and TBI treatments (Fig. 4E & 4F). The dose statistics are shown in Table 1 for 11 Gy TMI I, TMI I+4 and TBI treatment plans calculated on the same mice (n=5). The mean dose to the bone was within ±5% between TBI, TMI I and TMI I+4. Spleen dose was 11 Gy, kept at the prescription dose. The lung mean dose was reduced by 57% for TMI I and 37% for TMI I+4. The gut mean dose was reduced by 67% for TMI I and 53% for TMI I+4. Finally, the liver mean dose was reduced by 65% for TMI I and 52% for TMI I+4. About 40-60% of the volume of vital organs received less than 10% of the prescription (11 Gy) dose; however, the part of organs close to the placed beams in TMI I received a higher dose, thereby increasing the mean delivered dose to 30-40%. In TMI I+4, ~40% of the vital organs received at least 50% of the presciption dose. Therefore, the mean dose value needs to be cautiously considered for TMI planning. The simulated TBI and TMI treatment plans in the color wash are shown in Fig. 4G. Mice postion and weight had no impact on TMI dosimetry (Supplementary Table S3A, S3B). Comparison of preclinical TMI plan dosimetry to clinical results is shown in Fig. 4H. Mean dose reductions were observed for many sensitive organs (heart, lungs, liver, and gut), while a similar dose was maintained for the spleen and skeleton. The exception were the kidneys, which showed a relatively higher dose in preclinical model, due to their proximity to the spine. Future

development toward a multi-leaf collimator in preclinical treatment is expected to reduce radiation exposure to organs considering their size, shape and proximity to the target.

TMI maintains long-term engraftment with reduced organ damage

We asked whether the commonly known myeloablative TBI dose (~11 Gy in C57BL/6) was similar to TMI for survival. Interestingly, unlike TBI, where 11 Gy was completely lethal (median survival: 14 days), TMI 11 Gy prescribed dose to the target and avoidance of dose to the rest of the body (TMI I) was well tolerated and conferred survival for more than 100 days, indicating autologous recovery of BM. To determine the myeloablative dose for TMI, we increased the dose of TMI and found that TMI 14 Gy (median survival: 15 days) was lethal while TMI 12 Gy (median survival: 79 days) was sublethal (Fig. 5A). However, TMI (11 Gy) with a reduced body dose (4-6 Gy) was lethal (median survival: 12 days) (Fig. 5A). The survival of the mouse was similar whether the radiation was given in one single dose or in 2 factions 6h apart. The two-fraction regime was considered for rest of the study.

Next, we evaluated the effect of TMI on long-term engraftment in the congenic mouse BMT mouse model as mentioned in the methods, and the schema is shown (Fig. 5B). BLI based non-invasive assessment of donor cell engraftment shows that TMI I treated mice failed to engraft when 2 million donor BM cells was given, whereas TBI-treated mice engrafted successfully (Supplementary Fig. S3A). We hypothesized that since TMI 11 Gy dose to the bone marrow was not myeloablative more donor cells may be required to ensure engraftment. Increasing the donor BM cells to 5 million cells improved BM engraftment; however, engraftment was relatively lower than in TBI-treated mice (Fig. 5C **(ii)**). We also analyzed engraftment in mice treated with TMI and with a partial body dose. TMI with a body dose of 0 and 2 Gy (TMI I and TMI I+2) (Fig. 5C **(ii)**, Supplementary Fig S3B) had slightly reduced engraftment. However, a body dose of 4 Gy and 6 Gy (TMI I+4 and TMI I+6, respectively) ensured engraftment similar to TBI (Fig. 5C **(i, iii),** Supplementary Fig S3B). Therefore, we chose TMI I+4 for further study. Additionally, a further increase in the number of donor BM cells to 10 million showed ~90% engraftment in the peripheral blood of TMI I, TMI I+4 and TBI treated mice by ~10-12 weeks post BMT (Fig. 5D, Supplementary Fig S3C). The long-term engraftment analysis in the BM at 25 weeks post BMT showed that all mice groups engrafted donor BM cells similarly (Fig. 5E). A secondary BMT, using BM cells from the primary TBI, TMI I and TMI I+4 treated mice showed similar donor cell engraftment in PB and BM (Fig 5 F) in the secondary recipient mouse, suggesting similar long-term repopulating ability for all three groups.

In assessing post BMT acute gut damage, three days post BMT, TMI-treated mice gut showed mostly normal mucosal lining. The TBI treated mice mucosa shows villous blunting and crypt hyperplasia, as well as glandular drop out (Fig. 5G, H). The height of the villi is shorter in the TBI setting (blunting) (Fig. 5I) and there are fewer villi per area (drop out), relative to TMI. At the higher magnification (H&E, 200X magnification), the crypt in the TBI sample shows crowding of the crypt lining cells (Fig. 5G). This result clearly indicates that TMI, similarly to TBI, maintains suitable engraftment post BMT, however with the added advantage of reduced organ damage.

Discussion

Innovations of image-guided TMI have facilitated the exploration of precision radiation treatment as a conditioning regimen for BMT in hematological malignancies(8,13,15,16,28,35,36). However, a lack of a preclinical high-precision TMI model impedes mechanistic understanding and investigation of experimental therapeutics. We developed and comprehensively characterized a novel multimodal image-guided preclinical TMI 3D model and evaluated the impact of TMI in a congenic BMT model.

The described preclinical TMI development overcame several limitations by integrating several technological and computational advancements. The contrast enhanced whole body CT imaging and whole-body MRI were employed to obtain 3D anatomical details of target and vital organs. The CT-guided Monte Carlo dose calculations accounted for tissue heterogeneity, enhancing accuracy of organ dose evaluation. Furthermore, onboard CT imaging allowed geometric verification and adjustment of mice prior to treatment delivery to ensure accurate dose delivery. The 3D visualized dose distribution allowed for inspection and management of dose coverage to targets and vital organs. Additionally, anatomically specific volumetric information allowed generating organ-specific DVHs, a quantitative radiation parameter that could be experimentally varied to measure treatment response, organ-specific toxicities, and immune modulation. The relatively high dose to bone medium in mice during exposure to low energy (effective energy of 78.8 keV) x-ray (37,38) was because the photoelectric absorption in the bone medium is high (22). A sharp dose variation in the BM junction was evident from the dose simulation carried out using BM mimetic phantom and was corroborated with the dose profile generated from treatment across the femoral cross section (Fig. 3E–G). This 3D phantom, in future, will enable us to investigate differential effect of TMI on BM cells that are adhered to bone surface in comparison to cells in the marrow. Taken together, overall, our preclinical TMI model allowed a high-precision dose optimization for targets such as bone, bone marrow, and spleen and non-target vital organs including lungs, liver, and gut. Furthermore, dosimetric similarities and equivalence of our preclinical model to the clinical studies suggested that our model may be used for future clinically relevant investigations.

In the survival study, mice treated with TMI 11 Gy survived for more than 100 days, implying autologous BM recovery, while TBI 11 Gy was lethal. One possible explanation is that unexposed lymph nodes, liver, and other organs provide a supportive environment to BM cells (39) for autologous recovery after application of 11 Gy TMI. TBI and TMI delivered same dose (11 Gy) to bone marrow. Two days (~48h) post 11 Gy, both TMI and TBI treated mice showed significantly reduced BM cellularity (~10%) (Supplementary Fig S4A), suggesting early damage to BM was very similar. Furthermore, TMI significantly reduced organ dose (gut, liver, lung, etc.) (Fig 4F) compared to TBI. On the other hand, increasing TMI dose of up to 14 Gy ensured lethality in mice, despite reduced dose to organs. These data suggest that the lethality may be a compound effect of BM failure and organ damage. Next, we chose the TMI I and TMI I+4 models, with a range of radiation exposure organs from very low to high, for simplification and validation in BMT. We found that increased donor BM cells (up to 10 million cells) was required for successful donor engraftment in TMI I treatment. However, a partial body dose of 4-6 Gy in addition to 11

Gy to the BM ensured better engraftment. Therefore, these results warrant more studies to understand the role of various organs in BM recovery and long-term engraftment post BMT. Furthermore, TMI showed similar long-term engraftment as compared to TBI (Fig. 5D–F), and temporal profiling indicated donor engraftment was complete by 8 weeks and was stable over the long term (25 weeks). Therefore, the TMI model can be used as a high-precision preclinical radiation conditioning regimen, an alternative to TBI for bone marrow transplantation studies.

Our image guided TMI model could be potentially used for a range of scientific investigations: (i) RT dose escalation, complementing our ongoing clinical dose escalation strategy to study therapeutic benefit. (ii) Biological investigation of radiation effects on hematopoietic stems cells between TMI and TBI-treated mice. (iii) Lung pneumonitis and gut graft versus host disease (GVHD) are often associated with high radiation exposure(3,40). TMI reduced organ damage, particularly acute gut damage post BMT. Previous study suggests that an increased gut dose increases the severity of GVHD (40). Therefore, the GVHD mouse model in allogeneic BMT settings using TMI would enable us to further understand the role of radiation-induced gut damage in GVHD. (iv) A recent study using an anti-CD33-PET imaging modality showed that AML disease localizes mostly in the skeletal system and is highly heterogeneous (41). The PET-guided functional TMI (fTMI) could allow localized radiation boosts to sites of high disease burden to enhance increased tumor cell killing without damaging the entire skeletal system(11,42). (v) T-regulatory and T-conventional (Tregs/Tcon) based adoptive immunotherapy in conjunction with the TBI conditioning regimen has been optimized in patients with leukemia (12). However, relapse rates have remained unacceptably high in the setting of haploidentical HCT. The major advantage of BM-targeted TMI is to be able to treat with dose-escalated TMI to offer a strong antileukemic conditioning for patients who cannot tolerate TBI because of older age, or for younger patient populations with comorbidities (43). Additionally, it is also possible that TMI may reduce the rate of transplant related mortality (TRM) in younger patients while maintaining the antileukemic activity of TBI. This outcome has led to the initiation of Treg/Tcon together with TMI conditioning to enhance the antileukemic effect(44). Our preclinical model will enable in-depth understanding of how TMI conditioning in combination with adoptive immunotherapy reduces GVHD as well as maintaining a strong graft versus leukemia (GVL) effect. (vi) Furthermore, non-malignant hematological disorders (thalassemia and sickle cell disorders), are responsible for significant morbidity and mortality, representing a major global health problem. About 40-50% of patients have graft failure after allogeneic HCT(45), and increasing TBI conditioning from 2 Gy to 4 Gy significantly reduced graft failure(46). Multiple forms of organ damage are reported in adult patients with SCD(47). Therefore, it is anticipated that the TMI technology could adequately deliver high doses to the BM to improve engraftment, but with reduced radiation exposure to vital organs in order to decrease comorbidities associated with SCD.

There are several limitations to our first preclinical TMI 3D model. Treatment time is significantly longer than with TBI. Among several approaches, custom-built mouse holders, atlas-based automated contouring of target and organs, automated selection of the radiation field, and multi-leaf collimator-based intensity modulated radiation would help to reduce

the time needed for the treatment and would enhance precision dosimetry, which are being planned for further customization.

In conclusion, our novel preclinical image-guided 3D TMI model could be used as a new method for delivering radiation with high accuracy to geometrically and functionally complex targets, while reducing or sparing radiation to vital organs to preserve their functions. The model provides robust evidence of long-term engrafted BM and reconstitution ability. Thus, our new high-precision TMI preclinical model facilitates the reverse translation of clinical data to improve mechanistic studies and should lead to clinical development of potentially safe, effective, and durable therapeutic interventions for malignant and non-malignant hematological disorders.

Supplementary Material

Refer to Web version on PubMed Central for supplementary material.

Funding Statement:

Research reported in this publication is supported by the National Institutes of Health (2R01CA154491-01) (SH), and partly supported by ONCOTEST (Ghent, Belgium) (SH). The Small Animal Imaging Core at City of Hope is supported by P30CA033572.

Data Availability Statement for this Work

Research data are stored in an institutional repository and will be shared upon request to the corresponding author.

References:

1. Copelan EA. Hematopoietic stem-cell transplantation. New England Journal of Medicine 2006;354:1813–1826.
2. Thomas ED, Lochte HL, Cannon JH, et al. Supralethal whole body irradiation and isologous marrow transplantation in man. The Journal of clinical investigation 1959;38:1709–1716. [PubMed: 13837954]
3. Abugideiri M, Nanda RH, Butker C, et al. Factors influencing pulmonary toxicity in children undergoing allogeneic hematopoietic stem cell transplantation in the setting of total body irradiation-based myeloablative conditioning. International journal of radiation oncology, biology, physics 2016;94:349–59.
4. Ho VT, Weller E, Lee SJ, et al. Prognostic factors for early severe pulmonary complications after hematopoietic stem cell transplantation. Biology of blood and marrow transplantation : journal of the American Society for Blood and Marrow Transplantation 2001;7:223–9.
5. Salhotra A, Hui S, Yang D, et al. Long-term outcomes of patients with acute myelogenous leukemia treated with myeloablative fractionated total body irradiation tbi-based conditioning with a tacrolimus- and sirolimus-based graft-versus-host disease prophylaxis regimen: 6-year follow-up from a single center. Biology of blood and marrow transplantation : journal of the American Society for Blood and Marrow Transplantation 2020;26:292–299.
6. Kal HB, Loes van Kempen-Harteveld M, Heijenbrok-Kal MH, et al. Biologically effective dose in total-body irradiation and hematopoietic stem cell transplantation. Strahlenther Onkol 2006;182:672–9. [PubMed: 17072526]
7. Clift RA, Buckner CD, Appelbaum FR, et al. Allogeneic marrow transplantation in patients with acute myeloid leukemia in first remission: A randomized trial of two irradiation regimens. Blood 1990;76:1867–71. [PubMed: 2224134]

8. Hui SK, Kapatoes J, Fowler J, et al. Feasibility study of helical tomotherapy for total body or total marrow irradiation. Med Phys 2005;32:3214–3224. [PubMed: 16279075]
9. Stein A, Tsai N-C, Palmer J, et al. Total marrow and lymphoid irradiation (tmli) in combination with cyclophosphamide and etoposide in patients with relapsed/refractory acute leukemia undergoing allogeneic hematopoietic cell transplantation. European Society for Blood and Marrow Transplantation, accepted abstract 2019.
10. Duval M, Klein J, He W, et al. Hematopoietic stem-cell transplantation for acute leukemia in relapse or primary induction failure. Journal of clinical oncology 2010;28:3730. [PubMed: 20625136]
11. Sargur Madabushi S, Zuro D, SU Y-L, et al. Targeted marrow radiation (tmi) improves therapeutic efficacy of stat3 decoy molecules by augmenting its delivery and immune modulation in an ami mouse model. Blood 2019; 134:3929–3929.
12. Martelli MF, Di Ianni M, Ruggeri L, et al. Hla-haploidentical transplantation with regulatory and conventional t-cell adoptive immunotherapy prevents acute leukemia relapse. Blood, The Journal of the American Society of Hematology 2014;124:638–644.
13. Hui S, Brunstein C, Takahashi Y, et al. Dose escalation of total marrow irradiation in high-risk patients undergoing allogeneic hematopoietic stem cell transplantation. Biology of Blood and Marrow Transplantation 2017.
14. Patel PR, Rondelli D. Total marrow and lymphoid irradiation to rescue refractory leukemia. Biology of Blood and Marrow Transplantation 2017;23:536–537. [PubMed: 28192252]
15. Stein A, Palmer J, Tsai N-C, et al. Phase i trial of total marrow and lymphoid irradiation transplant conditioning in patients with relapsed/refractory acute leukemia. Biology of Blood and Marrow Transplantation 2017.
16. Rosenthal J, Wong J, Stein A, et al. Phase 1/2 trial of total marrow and lymph node irradiation to augment reduced-intensity transplantation for advanced hematologic malignancies. Blood 2011;117:309–315. [PubMed: 20876852]
17. Ma CM, Coffey CW, DeWerd LA, et al. Aapm protocol for 40-300 kv x-ray beam dosimetry in radiotherapy and radiobiology. Med Phys 2001;28:868–93. [PubMed: 11439485]
18. Hui S, Takahashi Y, Holtan SG, et al. Early assessment of dosimetric and biological differences of total marrow irradiation versus total body irradiation in rodents. Radiother Oncol 2017;124:468–474. [PubMed: 28778346]
19. Sengsayadeth S, Savani BN, Blaise D, et al. Reduced intensity conditioning allogeneic hematopoietic cell transplantation for adult acute myeloid leukemia in 19 complete remission - a review from the acute leukemia working party of the ebmt. Haematologica 2015;100:859–69. [PubMed: 26130513]
20. Andrade J, Ge S, Symbatyan G, et al. Effects of sublethal irradiation on patterns of engraftment after murine bone marrow transplantation. Biology of blood and marrow transplantation : journal of the American Society for Blood and Marrow Transplantation 2011;17:608–19.
21. Bachar-Lustig E, Rachamim N, Li H-W, et al. Megadose of t cell-depleted bone marrow overcomes mhc barriers in sublethally irradiated mice. Nature Medicine 1995;1:1268–1273.
22. Verhaegen F, van Hoof S, Granton PV, et al. A review of treatment planning for precision image-guided photon beam pre-clinical animal radiation studies. Zeitschrift fur medizinische Physik 2014;24:323–34. [PubMed: 24629309]
23. Willekens I, Buls N, De Maeseneer M, et al. Use of exia 160 xl for contrast studies in micro-computed tomography: Experimental observations. Molecular imaging 2013;12:349–56. [PubMed: 23981780]
24. Willekens I, Lahoutte T, Buls N, et al. Time-course of contrast enhancement in spleen and liver with exia 160, fenestra lc, and vc. Molecular imaging and biology : MIB : the official publication of the Academy of Molecular Imaging 2009;11:128–35.
25. van Hoof SJ, Granton PV, Verhaegen F. Development and validation of a treatment planning system for small animal radiotherapy: Smart-plan. Radiother Oncol 2013;109:361–6. [PubMed: 24183860]
26. Downes P, Jarvis R, Radu E, et al. Monte carlo simulation and patient dosimetry for a kilovoltage cone-beam ct unit. Med Phys 2009;36:4156–67. [PubMed: 19810489]

27. Faddegon BA, Kawrakow I, Kubyshin Y, et al. The accuracy of egsnrc, geant4 and penelope monte carlo systems for the simulation of electron scatter in external beam radiotherapy. Physics in medicine and biology 2009;54:6151–63. [PubMed: 19779217]
28. Aydogan B, Yeginer M, Kavak GO, et al. Total marrow irradiation with rapidarc volumetric arc therapy. International Journal of Radiation Oncology* Biology* Physics 2011;81:592–599.
29. Bao Z, Zhao H, Wang D, et al. Feasibility of a novel dose fractionation strategy in tmi/tmli. Radiat Oncol 2018;13:248. [PubMed: 30558631]
30. Han C, Schultheisss TE, Wong JY. Dosimetric study of volumetric modulated arc therapy fields for total marrow irradiation. Radiother Oncol 2012;102:315–320. [PubMed: 21724284]
31. Hui SK, Verneris MR, Higgins P, et al. Helical tomotherapy targeting total bone marrow - first clinical experience at the university of minnesota. Acta Oncol 2007;46:250–5. [PubMed: 17453378]
32. Jensen LG, Stiller T, Wong JY, et al. Total marrow lymphoid irradiation/fludarabine/melphalan conditioning for allogeneic hematopoietic cell transplantation. Biology of Blood and Marrow Transplantation 2018;24:301–307. [PubMed: 29032268]
33. Mancosu P, Navarria P, Castagna L, et al. Interplay effects between dose distribution quality and positioning accuracy in total marrow irradiation with volumetric modulated arc therapy. Med Phys 2013;40:111713. [PubMed: 24320421]
34. McCutchen KW, Watkins JM, Eberts P, et al. Helical tomotherapy for total lymphoid irradiation. Radiat Med 2008;26:622–6. [PubMed: 19132495]
35. Fogliata A, Cozzi L, Clivio A, et al. Preclinical assessment of volumetric modulated arc therapy for total marrow irradiation. International Journal of Radiation Oncology* Biology* Physics 2011;80:628–636.
36. Wong JYC, Liu A, Schultheiss T, et al. Targeted total marrow irradiation using three-dimensional image-guided tomographic intensity-modulated radiation therapy: An alternative to standard total body irradiation. Biology of Blood and Marrow Transplantation 2006;12:306–315. [PubMed: 16503500]
37. Chow J, Owrangi A. Su-e-t-142: Effect of the bone heterogeneity on the unflattened and flattened photon beam dosimetry: A monte carlo comparison. Med Phys 2014;41:255–255.
38. Bazalova M, Carrier JF, Beaulieu L, et al. Dual-energy ct-based material extraction for tissue segmentation in monte carlo dose calculations. Physics in medicine and biology 2008;53:2439–56. [PubMed: 18421124]
39. Johns JL, Christopher MM. Extramedullary hematopoiesis: A new look at the underlying stem cell niche, theories of development, and occurrence in animals. Veterinary pathology 2012;49:508–23. [PubMed: 22262354]
40. Hill GR, Crawford JM, Cooke KR, et al. Total body irradiation and acute graft-versus-host disease: The role of gastrointestinal damage and inflammatory cytokines. Blood 1997;90:3204–13. [PubMed: 9376604]
41. Srideshikan SM, Brooks J, Zuro D, et al. Immunopet, [(64)cu]cu-dota-anti-cd33 pet-ct, imaging of an aml xenograft model. Clin Cancer Res 2019;25:7463–7474. [PubMed: 31548348]
42. Magome T, Froelich J, Holtan SG, et al. Whole-body distribution of leukemia and functional total marrow irradiation based on flt-pet and dual-energy ct. Molecular imaging 2017;16:1536012117732203. [PubMed: 28948859]
43. Chao C, Bhatia S, Xu L, et al. Chronic comorbidities among survivors of adolescent and young adult cancer. J Clin Oncol 2020;38:3161–3174. [PubMed: 32673152]
44. Pierini A, Ruggeri L, Carotti A, et al. Haploidentical age-adapted myeloablative transplant and regulatory and effector t cells for acute myeloid leukemia. Blood Adv 2021;5:1199–1208. [PubMed: 33646302]
45. Bolanos-Meade J, Fuchs EJ, Luznik L, et al. Hla-haploidentical bone marrow transplantation with posttransplant cyclophosphamide expands the donor pool for patients with sickle cell disease. Blood 2012;120:4285–91. [PubMed: 22955919]
46. Bolanos-Meade J, Cooke KR, Gamper CJ, et al. Effect of increased dose of total body irradiation on graft failure associated with hla-haploidentical transplantation in patients with severe

haemoglobinopathies: A prospective clinical trial. The Lancet Haematology 2019;6:e183–e193. [PubMed: 30878319]

47. van Tuijn CFJ, Schimmel M, van Beers EJ, et al. Prospective evaluation of chronic organ damage in adult sickle cell patients: A seven-year follow-up study. Am J Hematol 2017;92:E584–e590. [PubMed: 28699283]

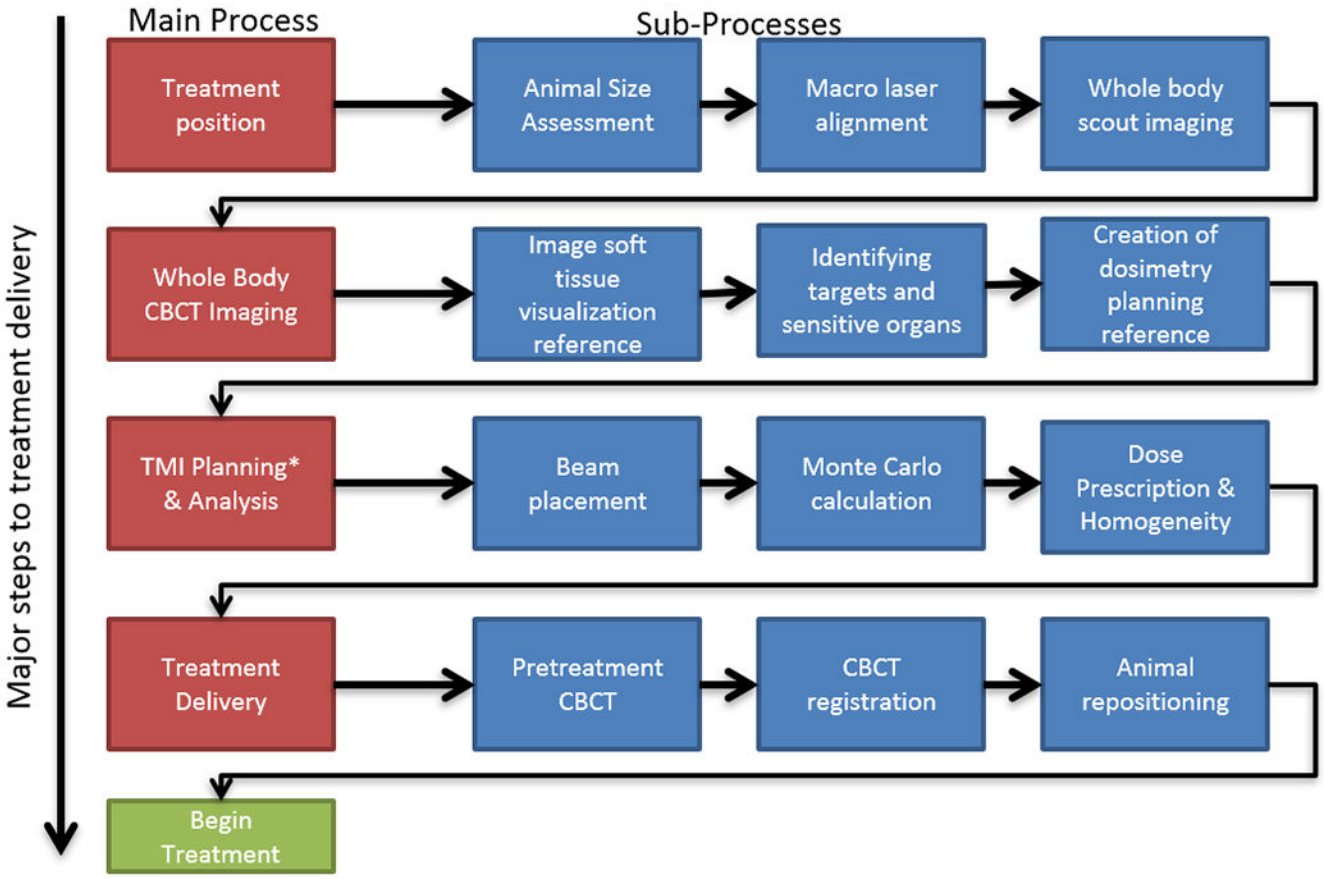

Figure 1: Workflow for a TMI treatment process.

The detailed step-by-step process for the TMI treatment is shown. Steps on the left in red are major steps. Steps in blue are sub-steps.

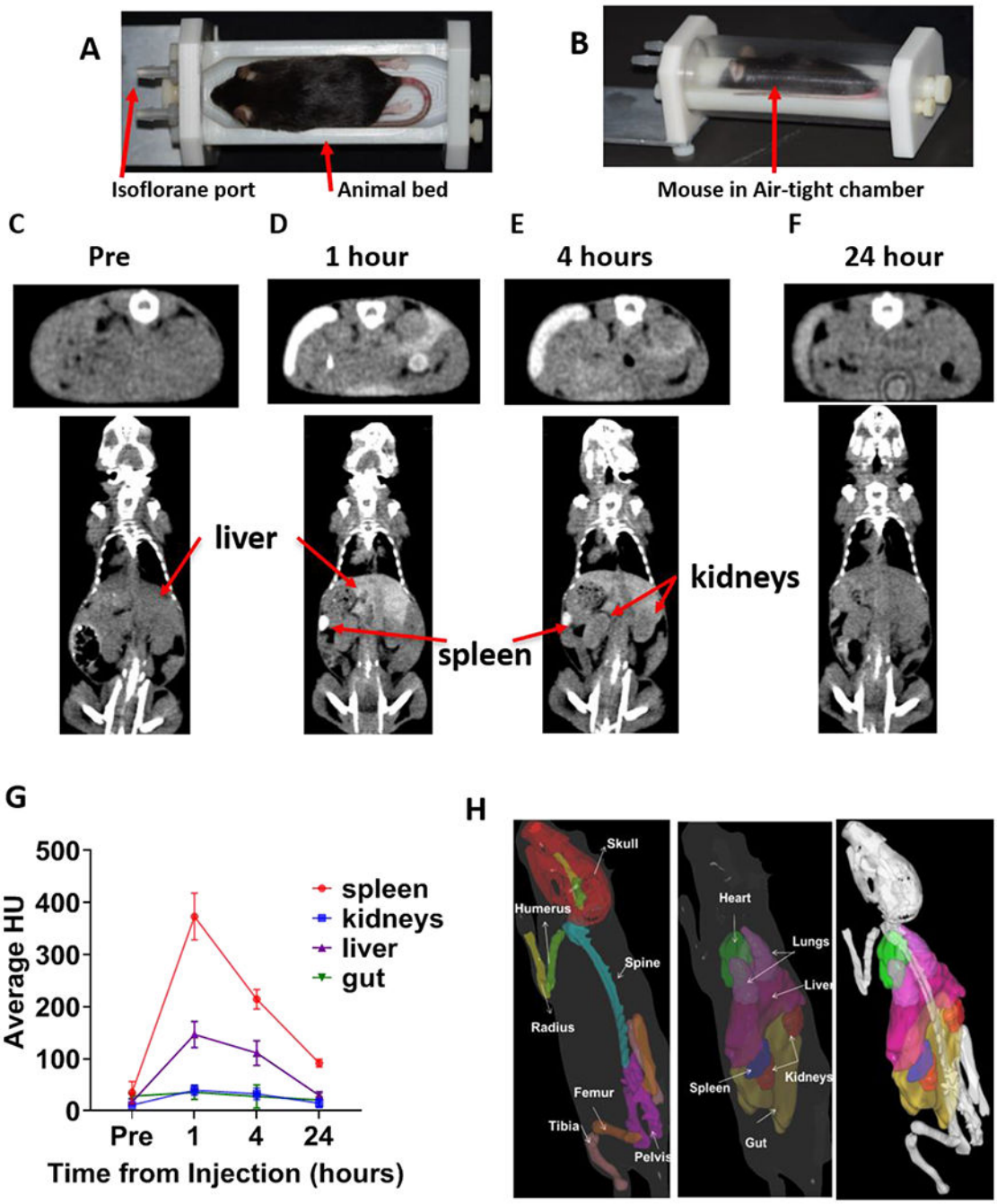

Figure 2: Pretreatment setup and Identification of soft tissues using the eXIA™ 160 contrast agent.

A) Custom-designed mouse holder base used in TMI treatment. **B)** Mouse placed in mouse holder chamber (base and transparent air-tight cylindrical chamber) to maintain continuous and homogeneous flow of isoflurane during TMI treatment delivery. **C-F)** The contrast agent eXIA™ 160 was injected via tail vein, and in vivo time-lapse CT imaging was carried out at different time points. Representative CT images taken at different time points are shown: **C)** prior to injection, **D)** 1h, **E)** 4h **F)** 24h after injection. **G)** The change in Hounsfield

Units over the course of 24h after injection is shown (n=5). **H)** Mouse contour (3D) showing skeletal tissue and vital organs, used in developing the TMI treatment plan.

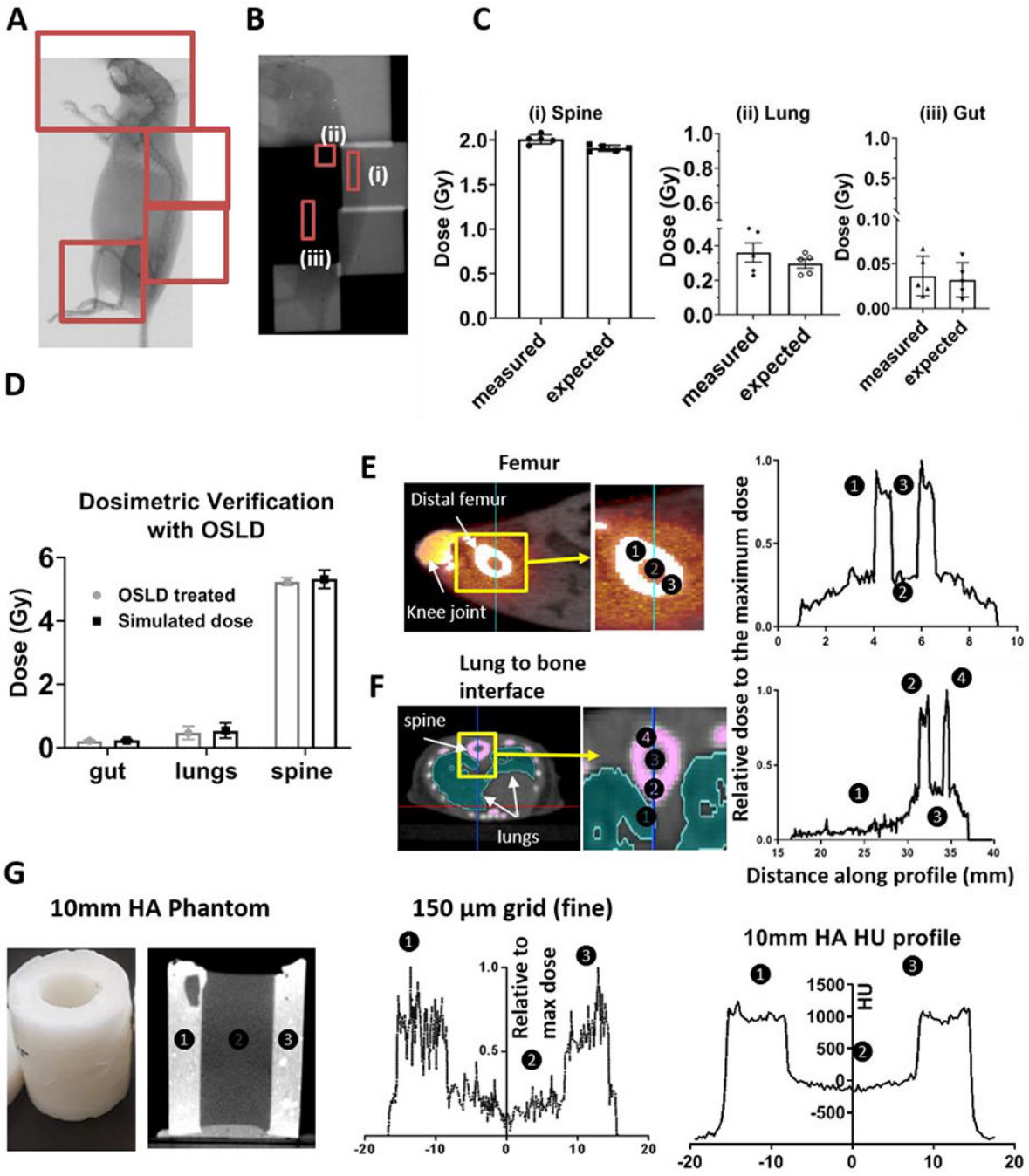

Figure 3: Dosimetric validation and dose profile simulation.

A) Fluorographic image displaying the animal position used for dosimetric verification with beam layout displayed in red. **B)** Gafchromic film used for dose verification (TMI dose delivered with 2 Gy) at three regions (spine (i), lungs (ii) and gut (iii) regions). **C)** Bar graphs displaying differences between measured and delivered dose to the Gafchromic film in spine, lungs and gut as identified in red in **B**. **D)** Bar graphs displaying differences between measured and delivered dose to the OSLD in same regions as described in B and C, delivered with 5 Gy. **E & F)** Visualized dose distribution location and corresponding

dose profile across bone, marrow, and surrounding tissue regions in femur (**E**) and spine (**F**) region are shown. The dose calculation was measured using Monte Carlo planning system with grid size of 150 μm, **G)** Bone and marrow mimetic phantom and dose profiles of this phantom filled with distilled water was measured using Monte Carlo planning system with dose calculation grid size of 150 μm with HU profile.

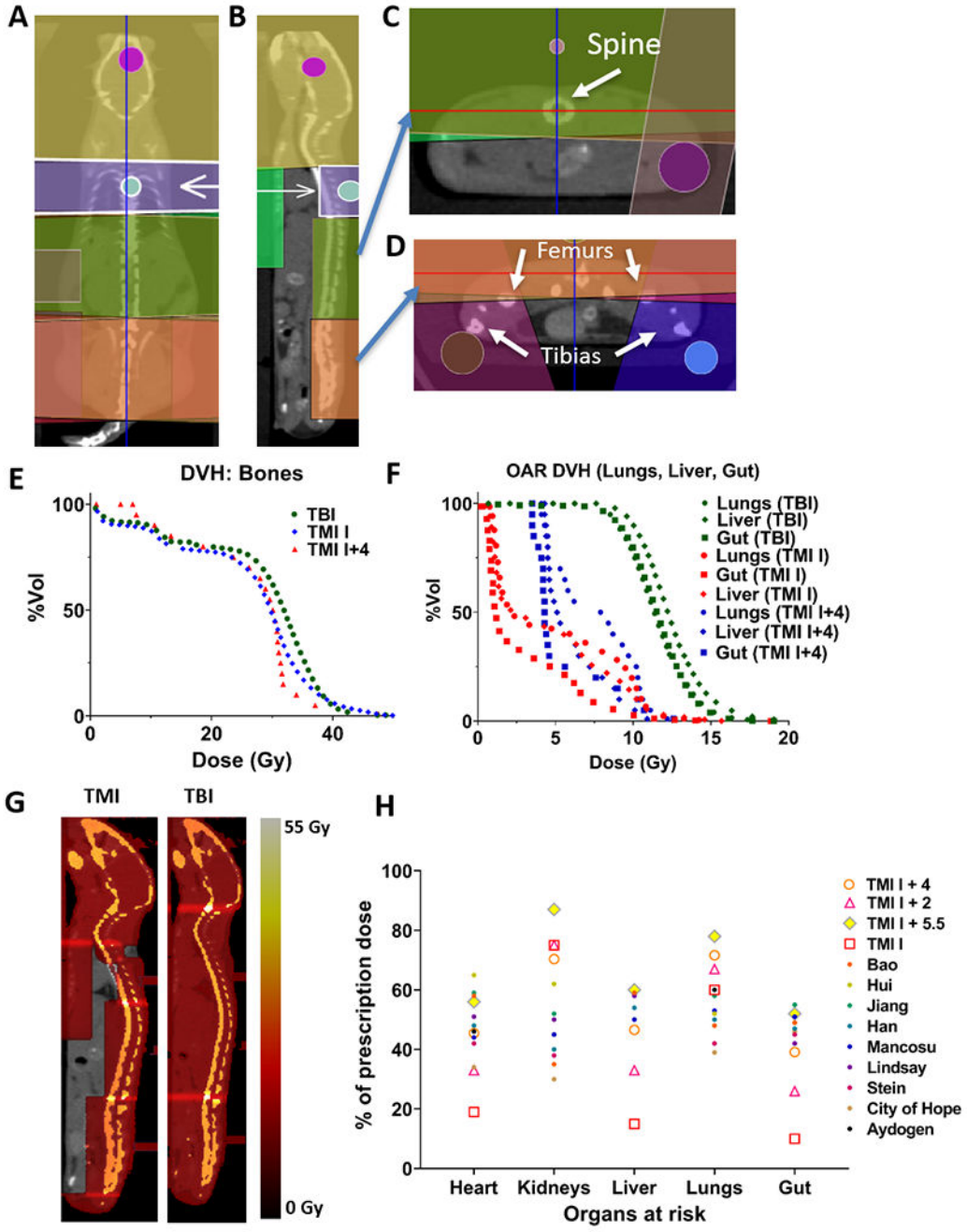

Figure 4: Common beam arrangements and dosimetry of TMI treatment.

Beam arrangement for parallel opposed beams in coronal view **(A)**, sagittal view demonstrating spine coverage **(B)**, axial view at spine with gut avoidance **(C)** and axial view at pelvis with leg beams **(D)**. A representative DVH comparing TMI and TBI plan for major organs viz., **(E)**, bones **(F)** gut, liver and lung. **G)** Visualized dose distribution of TMI and TBI plan. **H**) Preclinical and clinical dosimetric comparisons: Dosimetric comparison between TMI I, TMI I+2, TMI I+4, and TMI I+5.5 (n=5), and 10 clinical TMI cases.

Median dose difference represented as a percentage of the prescription dose. Regions of interest are the heart, lungs, liver, spleen, gut, kidneys, and target skeleton.

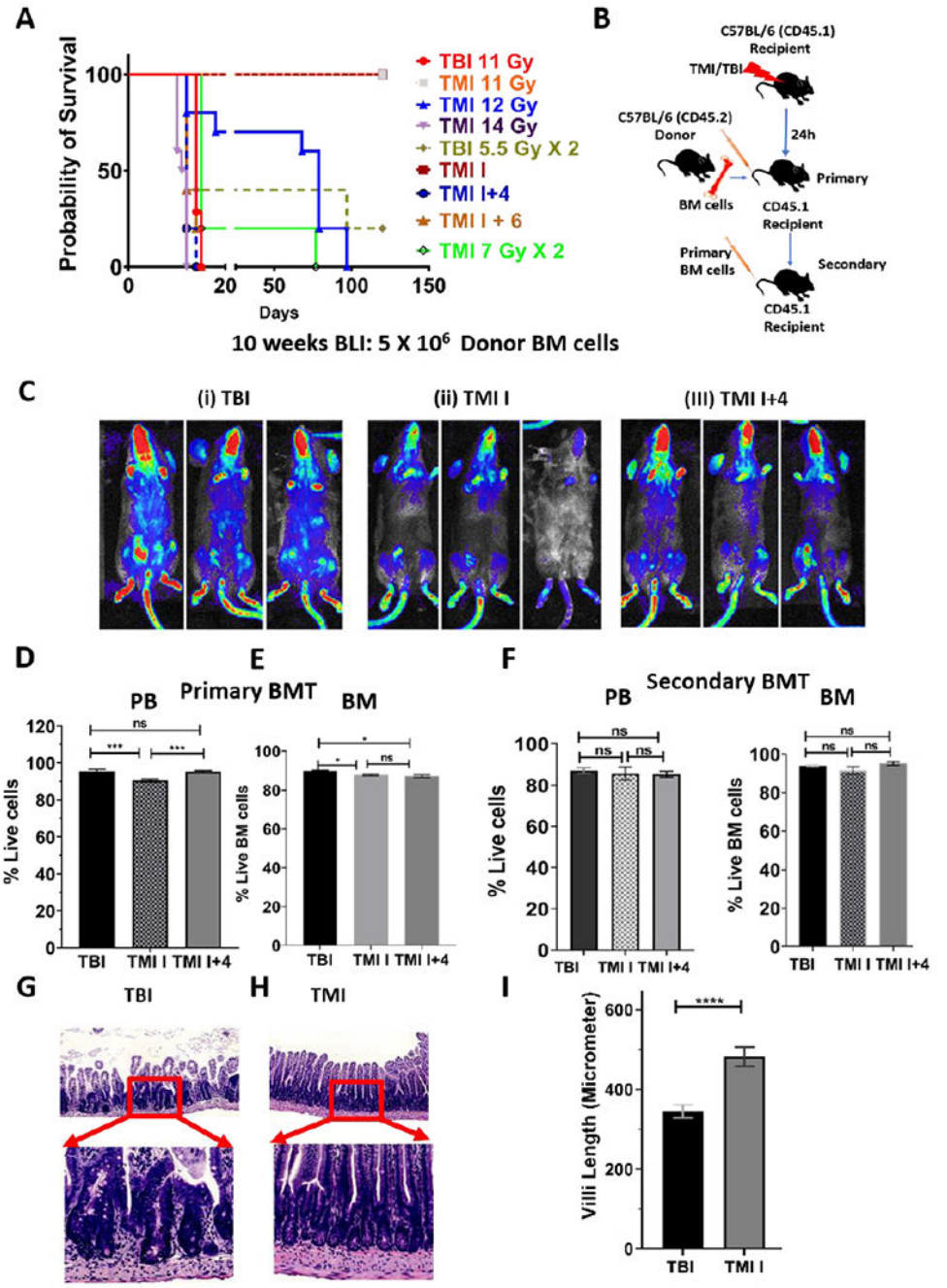

Figure 5: TMI myeloablative dose is higher than TBI and maintains long-term engraftment with reduced organ damage.

A) Survival curve showing that myeloablative dose of radiation for B6 mice was higher when radiation was delivered by TMI (14 Gy) than TBI (11 Gy). **B)** Schema of congenic primary and secondary bone marrow transplant (BMT) study. **C)** Donor cell engraftment in mice treated using different forms of TMI by varying doses to body (TMI I:0 Gy body; TMI I+4; 4 Gy body) in comparison to TBI treated mice. CD45.2 B6-Luciferase+ donor BM cell (5 million) engraftment 10 weeks post BMT by BLI. **D-E)** The donor cell engraftment

in peripheral blood (PB); 10 weeks post BMT **(D)** and BM **(E);** 25 weeks post BMT. **F)** Secondary BMT mouse showed similar donor engraftment in PB and BM between mice transplanted with primary BM cells from TBI, TMI I and TMI I+4 treated mice (n=5). **G-I)** Representative images of H&E-stained small intestine sections 3 days post BMT from TBI **(G)** and TMI I **(H)** treated mice. Enlarged portion of the small intestine showing blunting of villi and crypts hyperplasia in TBI treated mice while TMI treated mice showed normal gut morphology. **I)** Average villi length (micrometer) for TBI and TMI treated mice (n≥3 mice).

Table 1:
Dose comparison between TBI and TMI planning for a prescribed dose of 11 Gy.

A) The mean delivered dose to target (bone marrow, spleen) and organs (lungs, gut and liver) was determined for the TBI, TMI I and TMI I+4 treatment plans. The % reduction in dose delivered was calculated using the TBI-delivered dose to the respective organs as reference. There was a significant reduction of dose delivered to lung, liver and gut; however, dose delivered to bone marrow was similar between TBI, TMI I and TMI I+4 plans. **B-D)**The D95 **(B)**, D80 **(C)**, and D5 **(D)** for bones and other vital organs for TBI, TMI I and TMI I+4 plans. The dose values ± s.d was calculated for n=5 mice/group.

A)

Organ	TBI	TMI I		TMI I + 4Gy	
	Dmean (Gy)	Dmean (Gy)	% Dose difference from TBI	Dmean (Gy)	% Dose difference from TBI
Bone (PTV)	27.5 ± 1.2	27.8 ± 1.6	1.1	26.5 ± 1.5	−3.6
Lungs	12.0 ± 0.7	5.1 ± 0.9	−57.5	7.5 ± 0.8	−37.5
Gut	11.5 ± 0.1	3.8 ± 0.9	−67.0	5.4 ± 0.1	−53.1
Liver	12.6 ± 0.2	4.4 ± 0.5	−65.1	6.0 ± 0.8	−52.4

B)

Organ	TBI	TMI I		TM I + 4Gy	
	D95 (Gy)	D95 (Gy)	% Dose difference from TBI	D95 (Gy)	% Dose difference from TBI
Bone (PTV)	1.4 ± 0.7	2.6 ± 3.4	85.7	7.6 ± 3.7	442.8
Lungs	8.8 ± 0.4	1.0 ± 0.1	−88.6	4.1 ± 0.3	−60.0
Gut	8.6 ± 0.1	0.7 ± 0.1	−91.9	3.5 ± 0.1	−59.5
Liver	9.4 ± 0.1	0.9 ± 0.1	−90.4	4.3 ± 0.1	−53.8

C)

Organ	TBI	TMI I		TMI I + 4Gy	
	D80 (Gy)	D80 (Gy)	% Dose difference from TBI	D80 (Gy)	% Dose difference from TBI
Bone (PTV)	15.2 ± 3.1	19.6 ± 5.8	28.9	18.6 ± 4.3	22.4
Lungs	10.2 ± 0.5	1.5 ± 0.3	−85.3	4.5 ± 0.2	−55.9
Gut	10.0 ± 0.1	0.9 ± 0.1	−91.0	3.9 ± 0.2	−61.0
Liver	10.8 ± 0.1	1.3 ± 0.1	−88.0	4.4 ± 0.2	−58.3

D)

Organ	TBI	TMI I		TMI I + 4Gy	
	D5 (Gy)	D5 (Gy)	% Dose difference from TBI	D5 (Gy)	% Dose difference from TBI
Bone (PTV)	40.2 ± 1.1	40.7 ± 2.9	1.2	37.1 ± 5.2	−7.7
Lungs	15.7 ± 1.3	11.3 ± 0.6	−28.0	11.1 ± 0.7	−29.3
Gut	14.6 ± 0.1	10.8 ± 0.9	−26.0	10.7 ± 0.2	−26.7
Liver	17.6 ± 1.3	11.3 ± 1.4	−35.8	10.1 ± 0.6	−42.6